# Femtochemistry of the Hydrated Electron at Decimolar Concentration

**S. Pommeret,*,†,‡ F. Gobert,‡,§ M. Mostafavi,§ I. Lampre,§ and J.-C. Mialocq‡**

*CEA/Saclay, DSM/DRECAM/SCM URA 331 CNRS, 91191 Gif-sur-Yvette Cédex, France, and Laboratoire de Chimie Physique UMR 8000, CNRS/Université Paris-Sud, Centre d'Orsay, Bâtiment 349, 91405 Orsay Cedex, France*

*Received: June 19, 2001; In Final Form: September 21, 2001*

We report a femtosecond laser study of the transient absorption of hydrated electrons generated by 266 nm two-photon ionization of liquid water under very high power laser density (up to 1.5 TW/cm$^2$). The two-photon absorption coefficient of liquid water for femtosecond pulses at 266 nm was determined to be $\beta = (1.8 \pm 0.4) \times 10^{-11}$m/W. The quantum yield of formation of the hydrated electron per absorbed photon at 266 nm is determined to be $0.26 \pm 0.02$. We observed, for the first time, that the decay of the hydrated electron produced under 1.5 TW/cm$^2$ laser pump power density in pure water is not only due to geminate recombination and that the survival probability of the hydrated electron at 1 ns is $0.16 \pm 0.02$ under those conditions, where an unprecedented local concentration of the hydrated electron of 0.15 M is produced.

## Introduction

In radiation chemistry, the study of the reactivity of very highly concentrated hydrated electrons is of primary importance. Indeed, following high-energy deposition, the primary products of water radiolysis are formed in tracks of limited volumes called spurs.[1−3] Those radiolytic species with high local concentrations of about 0.1 mol dm$^{-3}$ undergo very fast processes of thermalisation, solvation, and recombination within the spurs.[2,3] Over the past few decades, the elucidation of the primary processes at times closer and closer to the moment of energy deposition has been made possible using picosecond pulse radiolysis[4,5] and femtosecond laser spectroscopy.[6,7] Due to the lack of pulse radiolysis facilities with time resolution shorter than a few tens of picoseconds, studies of the ultrafast processes have been indeed conducted with femtosecond lasers. Those studies showed that the interaction of intense laser pulses with neat water produces hydrated electrons, hydroxyl radicals, hydrogen atoms, and hydronium cations via multiphoton absorption mechanisms[6−9] (Figure 1). Among the generated species, the hydrated electron has been studied extensively and in detail. Hydrated electron, hydrogen atom, and hydroxyl radical all weakly absorb in the UV, but only the hydrated electron presents a large and intense absorption band peaking at 718 nm.[1,10,11] Recently, pump−probe laser spectroscopy studies of neat water at very short times gave evidence that several precursors of the hydrated electron absorbing mostly in the infrared domain exist and that the hydration process is complete within few hundreds of femtoseconds.[7] Subsequent geminate recombinations[8,9,12,13] between hydrated electrons ($e^-_{aq}$) and hydronium cations or hydroxyl radicals occur on the picosecond time scale (reactions 1 and 2).

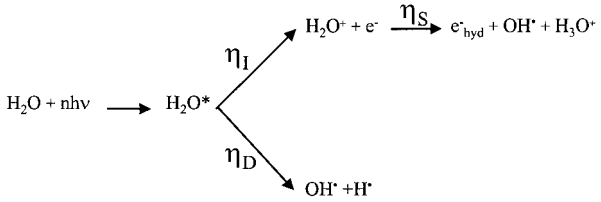


**Figure 1.** Schematic view of the primary events following the simultaneous absorption of n photons. $\eta_I$ is the quantum yield of ionization per absorbed photon, $\eta_S$ is the quantum yield of electron solvation per ionization, and $\eta_D$ is the quantum yield of dissociation per absorbed photon.

$$e_s^- + H_3O^+ \rightarrow H^\bullet + H_2O \qquad k_1 = 2.3 \times 10^{10}\ \mathrm{dm^3\ mol^{-1}\ s^{-1}}\ ^{14} \quad (1)$$

$$e_s^- + OH^\bullet \rightarrow OH^- \qquad k_2 = 3.0 \times 10^{10}\ \mathrm{dm^3\ mol^{-1}\ s^{-1}}\ ^{14} \quad (2)$$

This early reactivity has been described with the help of the independent pair model[15] (see the fitting of the experimental data in refs 8, 9, 15, 16). In pure water, the transient radicals formed through the reaction scheme shown in Figure 1 last until the microsecond range. However, in the presence of high solute concentrations, the hydrated electron and also its precursors can be scavenged with a rate which depends on the nature of the solute. A wealth of experimental data exists on the rate constants of the hydrated electron with various solutes.[14,17] But because the lifetimes of the precursors are very short, only a few data on the scavenging of those precursors are reported.[18] For example, cadmium, selenate, and nitrate are known to be strong scavengers of the hydrated electron precursors.[18−22]

Recently, we have reported nanosecond transient absorbance data following the multiphoton excitation of water by powerful femtosecond laser pulses centered at 266 and 400 nm.[23] We suggested that under pump power densities higher than 1 TW/cm$^2$, the initial distribution of hydrated electrons along the water jet thickness should be highly nonuniform. To determine the initial spatial distribution profile of the hydrated electron and to unravel its early reactivity,[24] we present

* To whom all the correspondence should be addressed. E-mail: Stanislas.Pommeret@cea.fr.

† Present address: Argonne National Laboratory, 9700 South Cass Avenue, Argonne, Il 60439, USA. Stanislas.Pommeret@anl.gov.

‡ CEA/Saclay, DSM/DRECAM/SCM URA 331 CNRS.

§ Laboratoire de Chimie Physique UMR 8000, CNRS/Université Paris-Sud.

10.1021/jp0123381 CCC: $20.00 
Published on Web 11/29/2001

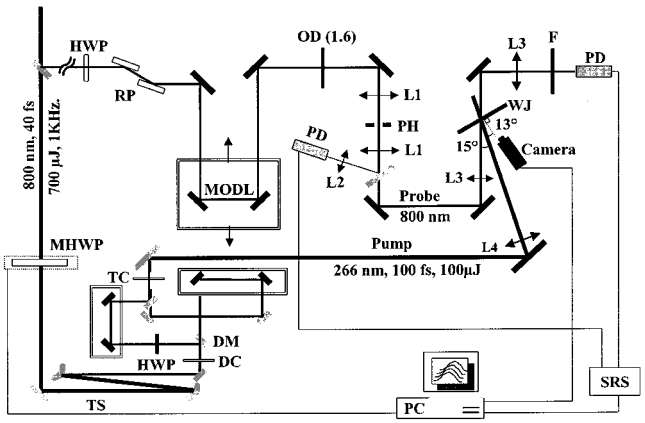


**Figure 2.** Femtosecond pump−probe experimental setup. Lenses: L1 ($f = 50$ mm), L2 ($f = 200$ mm), L3 ($f = 100$ mm), L4 ($f = 500$ mm). PD, photodiode; PH, pinhole; RP, reflective polarizer; F, RG610 Schott filter; (M)HWP, (motorized) half-wave plate; OD, neutral optical density; MODL, motorized optical delay line; DC, doubling crystal (BBO type I, 0.2 mm); TC, tripling crystal (BBO type I, 0.1 mm); TS, reflective telescope.

femtosecond transient absorption results obtained by exciting water at 266 nm with a very high power density laser pump. In the first part of the paper, we depict the kinetics obtained in the absence and in the presence of scavengers. We then analyze the two-photon absorption under our experimental conditions, and finally, using the concentration profile of the absorbed photons, we show that the hydrated electron can be produced up to a decimolar concentration by increasing the laser power density while so far, only submillimolar concentrations of radicals were produced under femtosecond laser excitation.[6−9]

## Experimental Section

To produce high concentrations of hydrated electron and to investigate its subsequent reactivity, femtosecond pump−probe transient absorption experiments were performed using a commercial kilohertz Ti:Sa laser system.[25] The experimental setup is shown in Figure 2. The main experimental difficulties were to control the pump power density and to ensure an extremely good overlap between the pump (266 nm) and probe (800 nm) beams. Indeed, the buildup of high concentrations of hydrated electron induces strong transient absorbances ($\Delta A >$ 1) which are difficult to measure accurately. To increase the pump power density, the pump beam has to be cautiously focused in the 70 $\mu$m thick water jet. The full width at half-maximum (fwhm) beam diameter was usually set to 180 $\mu$m, and the pump beam energy was varied using a motorized half-wave plate.[26] Because the probe beam has not an ideal Gaussian profile when tightly focused, wings containing a few percent of the overall probe pulse energy were observed. To avoid the wings, the probe beam was first spatially filtered using a 50 $\mu$m pinhole inside a Keplerian beam expander (magnification of 1 and overall length of 0.4 m), and then it was focused onto the water jet using a 100-mm-focal-length lens. The measured probe beam diameter was less than 50 $\mu$m fwhm (Figure 2). The intensities of the probe and reference beams were measured using silicon photodiodes. The signals were then digitized using a boxcar (SRS Instruments). For the nonlinear transmission experiment, the incident pump energy was measured just after the focusing lens, and the transmitted energy was measured after the water jet. All the beam diameters (fwhm) were measured using a CCD camera (COHU). The pulse duration of the 266 nm pulse was determined either by measuring the rise time of the ferricyanide[25] or by the photobleaching of laser dyes.[27] The duration of the 266 nm laser pulse was 100 ± 20 fs fwhm.

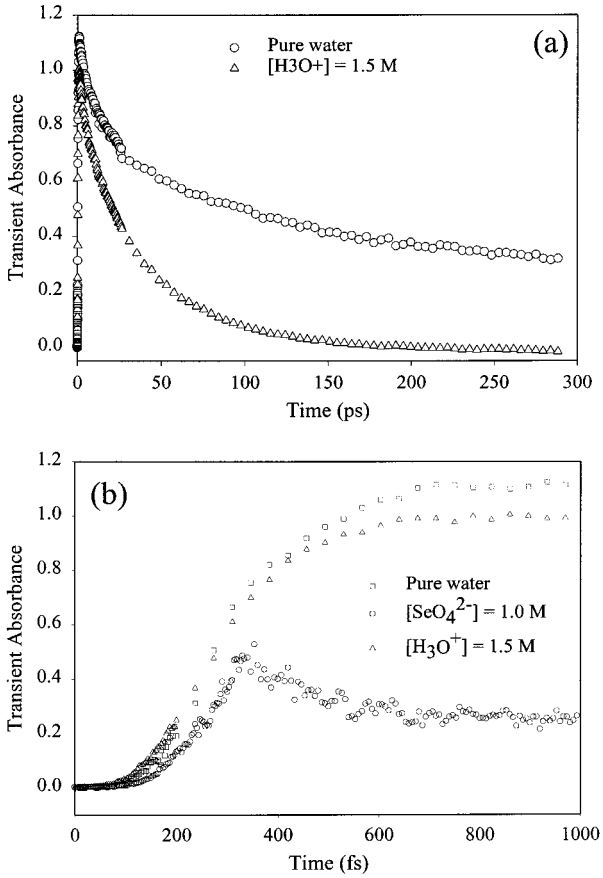


**Figure 3.** Transient kinetics measured at 800 nm after the photoexcitation of aqueous solutions at 266 nm with a power density of 1.5 TW/cm$^2$ ((a) picosecond experimental data; (b) femtosecond experimental data).

The flow of the water jet was fast enough to ensure a complete renewal of the sample between two laser pulses (1 ms). Due to the high quality of the sapphire nozzle (Victor Kyburz AG), it was possible to obtain a stable laminar water flow at room-temperature despite the low viscosity of water. Water was deionized in a Waters Millipore apparatus to a resistivity greater than 18 MΩ cm and acidified using perchloric acid (Merck). The perchlorate anion is considered inert with respect to electron photodetachment in the near UV and does not react with the hydrated electron, the hydroxyl radical and the hydrogen atom.[28] Sodium selenate decahydrate (Aldrich) was used as received.

## Results and Discussion

**Formation and Decay of the Hydrated Electron.** Figure 3 displays for comparison the ultrafast transient absorbances measured at 800 nm in pure water and in aqueous solutions strongly acidic (0.75 M $HClO_4$) or with a 1 M concentration of selenate ($Na_2SeO_4$) after a powerful laser excitation at 266 nm. The very strong transient absorbances recorded in pure and strongly acidic water at early times must be emphasized (Figure 3a). In pure water, less than 30% of the initial absorbance ($\Delta A$ = 1.1) still remains after 300 ps, while in strongly acidic solution, it disappears totally within the same time scale. The comparison of these two decays is in line with the assignment of the 800 nm absorbance to the hydrated electron and literature findings concerning its scavenging by the hydronium cation on

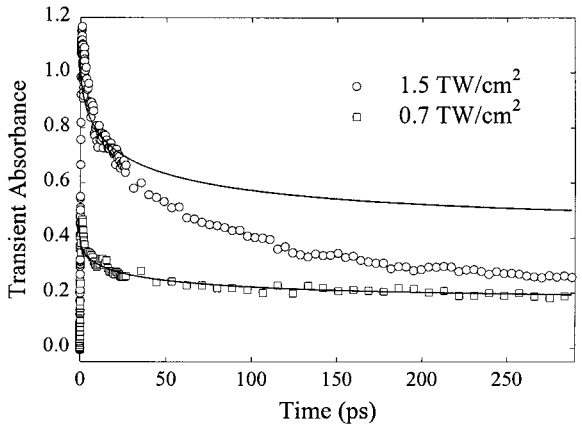


**Figure 4.** Effect of the pump power density (266 nm) on the kinetics traces of the hydrated electron recorded at 800 nm in pure water (squares, 0.7 TW/cm$^2$; circles, 1.5 TW/cm$^2$). The full lines correspond to the kinetic law used to fit the geminate recombination as proposed in ref 9; the curves are scaled to fit the data around $t = 10$ ps.

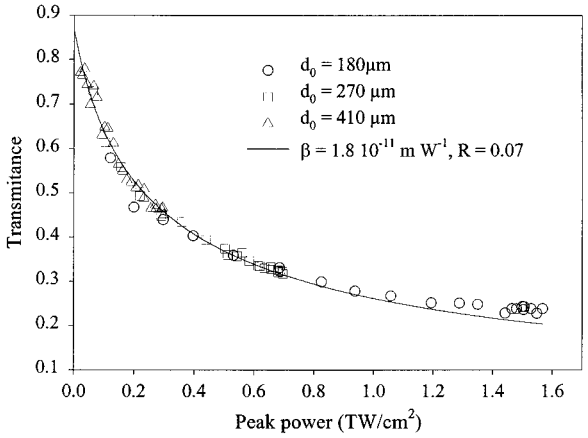


**Figure 5.** Two-photon absorption in neat water at 266 nm. The transmittance of the 70 $\mu$m water jet is plotted vs the peak power of the 100 fs input pulse (symbol: experimental data for three different pump diameters; solid line calculated curve).

the picosecond time scale.[29] Indeed, in the strongly acidic solution, the 800 nm decay is well fitted for times longer than 10 ps by a single-exponential decay with a time constant of 40 $\pm$ 1 ps. From this pseudo-first-order decay, the second-order rate constant of the reaction of the hydrated electron with the hydronium cation is found to be $k = 1.7 \times 10^{10}$ mol$^{-1}$ dm$^3$ s$^{-1}$, a value in agreement with those reported in the literature.[14,30] Whereas the initial transient absorption in the strongly acidic aqueous is slightly lower (about 10%) than that observed in pure water (Figure 3b), in the presence of selenate (Figure 3b), the observed transient absorbance is strongly reduced. Indeed, the latter signal exhibits a maximum around $t = 300$ fs and then decays, while the transient absorbances measured in pure water and in the acidic solution rise and reach a maximum at $t = 600$ fs (Figure 3b). It is to be remembered that the hydrated electron and its precursors all absorb at 800 nm,[7] and it is well-known that in contrast to the hydronium cation, the selenate ion scavenges the precursors of the hydrated electron efficiently and the hydrated electron poorly.[18,22,31−33] The yield of the hydrated electron at 1 ps in the presence of 1 M selenate is reduced by a factor of 5 with respect to that in pure water (Figure 3b). Consequently, the present results show that, under such unprecedented high laser pump power densities, the signals observed at 800 nm are not issued from an optical artifact, but they are due to the absorption of the hydrated electron. At very short time, the signals are partly due to precursors of the hydrated electron as previously reported.[7]

The change in the pump power density affects not only the maximum absorbance, but also the kinetics (Figure 4). The kinetics recorded for two excitation power densities (1.5 and 0.7 TW/cm$^2$) are compared to the geminate recombination kinetics on the basis of the independent pair approximation[15] already used to fit experimental data at low excitation power density.[8,9,16] Interestingly, although the experimental decay kinetics obtained for 0.7 TW/cm$^2$ is well fitted from 10 to 300 ps using the independent pair approximation, the kinetics obtained at 1.5 TW/cm$^2$ cannot be fitted similarly. Particularly, the decay observed at long times is much faster. It might be related to the relatively high concentrations of the radicals. At high laser power density, the measured absorbance ($\Delta A \geq 1$) at 800 nm ($\epsilon_{800} = 15\,700$ mol$^{-1}$ dm$^3$ cm$^{-1}$)[10,11] corresponds to an average hydrated electron concentration of about 0.01 M over the entire 70 $\mu$m thick water jet. Such a high hydrated electron concentration has never been reported. However, this is an underestimate of the peak concentration because this simple calculation does not account for the real depth-dependent concentration produced inside the water jet, which results from nonlinear absorption of the 266 nm laser beam. To estimate the real peak concentration, we performed nonlinear transmittance experiments described in the following section.

**Two-Photon Absorption at 266 nm.** The transmittances measured as a function of the 266 nm laser intensity gathered in Figure 5 are characteristic of a single-beam two-photon absorption (SB-TPA).[6,8,13,34,35] If simultaneous absorption of two photons is the only process involved, the change of irradiance $I(z,r,t)$ ($z$, $r$, and $\theta$ are the cylindar coordinates) along the optical path length $z$ is given by:[6,13,26,34,35]

$$\frac{1}{I(z,r,t)}\frac{\partial I(z,r,t)}{\partial z} = -\beta_2 I(z,r,t) = (N_g - N_e)\sigma_2\left(\frac{I(z,r,t)}{h\nu}\right) \quad (3)$$

where $\beta_2$ and $\sigma_2$ are the SB-TPA coefficient and cross section, respectively, $h\nu$ is the energy of the incident photon, and $N_g$ and $N_e$ are the population densities in the ground and excited states, respectively. The SB-TPA coefficient $\beta_2$ is a material-dependent macroscopic parameter expressed in units of m W$^{-1}$, while the SB-TPA cross section $\sigma_2$ is a molecular property expressed in units of m$^4$ s. In the following, we assume that the incident pulse shape $I_0(r,t)$ is given by Gaussian functions in time ($t$) and in transverse coordinate ($r$):

$$I_0(r,t) = I_0 \exp\left(-4\ln(2)\frac{r^2}{{d_0}^2}\right)\exp\left(-4\ln(2)\frac{t^2}{{t_0}^2}\right) \quad (4)$$

where $t_0$ is the pulse duration (fwhm), $d_0$ the beam diameter (fwhm), and $I_0$ the peak irradiance. The total energy $E_0$ contained in the incident pulse is obtained by integrating $I_0(r,t)$ over the time and transverse coordinates. This leads to the following relation between the peak irradiance $I_0$ and the pulse energy $E_0$:

$$I_0 = \left(\frac{4\ln(2)}{\pi}\right)^{3/2}\frac{E_0}{t_0{d_0}^2} \quad (5)$$

When a pulsed laser source is used, the transmittance ($T$) is given by the ratio of the transmitted pulse energy $E$ to the incident pulse energy $E_0$. Integrating eq 3 gives:

$$T = \frac{E}{E_0} = \frac{(1-R)^2}{E_0}\int_0^{\infty} \mathrm{d}r\, 2\pi r \int_{-\infty}^{\infty} \mathrm{d}t \frac{I_0(r,t)}{[1+\beta_2 L(1-R)I_0(r,t)]} \quad (6)$$

where $R$ denotes the Fresnel reflection losses at the air−water and water−air interfaces and $L$ is the water jet thickness. We have fitted our experimental values of the transmittance ($T$) as a function of the peak irradiance ($I_0$) with a SB-TPA process (eq 6). The best fit of the data is obtained for $\beta_2 = 1.8 \times 10^{-11}$ m W$^{-1}$ and $R = 0.07$[32] (Figure 5). The present value of $\beta_2$ obtained at 266 nm is 18 times higher than the literature value obtained in a picosecond experiment[6] (Table 1). Note that as shown in Appendix I the error on the $\beta_2$ value is quite large. In Table 1, we also report the value of Reuther et al.[13] We remark that the $\beta_2$ values obtained with ultrashort laser pulses are larger than those obtained with picosecond pulses.

**TABLE 1: Comparison of the Values of the Two-Photon Absorption Coefficients of Water at Various Wavelengths**

| $\lambda$ (nm) | $t_0$ (ps) | $\beta_2$ ($10^{-12}$ m/W) | $\sigma_2$ ($10^{-58}$ m$^4$ s) | ratio | reference |
|---|---|---|---|---|---|
| 266 | 0.1 | $18 \pm 4$ | 3.9 | $\beta_2(266\text{nm})/\beta_2(282\text{nm}) = 9 \pm 4$ | this work |
| 282 | 0.18 | $1.9 \pm 0.5$ | 0.42 | | 13 |
| 266 | 18 | 1 | 0.22 | $\beta_2(266\text{nm})/\beta_2(281\text{nm}) = 1.4$ | 6 |
| 281 | 18−23 | 0.7 | 0.15 | | 6 |

To justify our result, it is worthwhile to estimate the ratio of the SB-TPA coefficient at 266 nm and at 282 nm using the recently published two-beam TPA (TB-TPA) spectrum (experimental and theoretical) of water in the UV spectral domain (see Figure 4 of ref 9). Indeed, as shown in Appendix II, there is an approximate relation between the TB-TPA spectrum and the measured SB-TPA coefficients:

$$\xi = \frac{\Delta A(\lambda_1)}{\Delta A(\lambda_2)}\frac{\beta_{\lambda_3,\lambda_3}}{\beta_{\lambda_1,\lambda_1}} \approx 1 \quad (7)$$

where $\Delta A(\lambda_i)$ is the measured maximum transient absorbance at $\lambda_i$ with a pump at $\lambda_1$, $\beta_{\lambda i,\lambda i}$ is the SB-TPA coefficient at $\lambda_i$, and the wavelengths satisfy $1/\lambda_1 + 1/\lambda_2 = 2/\lambda_3$ ($\lambda_1 = 266$ nm, $\lambda_2 = 300$ nm and $\lambda_3 = 282$ nm). Using the numerical values of ref 9 for the $\Delta A$ ($\Delta A(266\text{ nm}) = 0.7 \pm 0.1$ and $\Delta A(300\text{ nm}) = 0.15 \pm 0.05$), we find for the ratio of the SB-TPA coefficients:

$$\frac{\beta(266\text{nm})}{\beta(282\text{nm})} \approx 5 \pm 2 \quad (8)$$

This value is smaller but compatible within the experimental uncertainties with the ratio ($9 \pm 4$) of the $\beta$ values experimentally measured at 266 nm and at 282 nm (see Table 1). It is clear that the $\beta$ values of Nykogosyan et al.[6] underestimate the sharp rise of the SB-TPA near 266 nm.

It is also worthwhile comparing the SB-TPA cross section at 266 nm and the three-photon absorption cross section at 400 nm. According to Naskrecki et al.,[26] the three-photon absorption cross section at 400 nm is $\sigma_3(400\text{ nm}) = 6.7\ 10^{-93}$ m$^6$ s$^2$. Thus, the ratio $\sigma_3(400\text{ nm})/\sigma_2(266\text{ nm}) = 1.7 \times 10^{-35}$ m$^2$ s is in agreement with the ratios obtained for other compounds.[37−40]

**Multiphoton-Absorption Profile and Hydrated Electron Concentration.** The amount of energy absorbed per unit of time and volume (irradiance deposit distribution IDD($z,r,t$)) can be derived from eq 3, neglecting the deformation of the propagating pulse:

$$\mathrm{IDD}(z,r,t) = -\frac{\partial I}{\partial z}(z,r,t) = (1-R)^2\beta_2\frac{I_0^2(r,t)}{[1+\beta_2 z(1-R)I_0(r,t)]^2} \quad (9)$$

the notations are identical to the ones of eqs 3−7, and $z$ ranges from 0 to $L$. Dividing by the photon energy ($h\nu$) and integrating over time, one can deduce the profile of absorbed photons per pulse $C(z,r)$:

$$C(z,r) = \frac{1}{h\nu N_A}\int_{-\infty}^{+\infty}\mathrm{IDD}(z,r,t)\,\mathrm{d}t \quad (10)$$

where $N_A$ is the Avogadro number. According to eqs 4, 9, and 10, $C(z,0)$ is the maximum longitudinal concentration profile (MLCP) of absorbed photons along the water jet. The MLCP($z$) and the mean radial concentration profile (MRCP) of absorbed photons, MRCP($r$), functions are defined by eq 11:

$$\begin{cases}\mathrm{MLCP}(z) = C(z,0) \\ \mathrm{MRCP}(r) = \dfrac{1}{L}\displaystyle\int_0^L C(z,r)\,\mathrm{d}z\end{cases} \quad (11)$$

Figure 6 shows the two concentration profiles defined in eq 11 using the $\beta_2$ and $R$ values determined in the previous section ($\beta_2 = 1.8 \times 10{-}11$ m/W, $R = 0.07$), the peak power density $I_0 = 1.5$ TW/cm$^2$, and the pump beam diameter $d_{\mathrm{pump}} = 180\ \mu$m. We remark that the MRCP almost matches the pump pulse profile (Figure 6a). This is indeed not surprising since at very high irradiance more than 70% of the pump pulse energy is absorbed by the sample (Figure 5). Therefore, the probe pulse ($d_{\mathrm{probe}} = 50\ \mu$m) probes only a very limited area of the excited region characterized by a nonuniform radial absorbance profile ($A(r,t)$). As shown in the section "formation and decay of the hydrated electron", the measured absorbance $\Delta A_{\mathrm{mes}}(t)$ is dominated by the absorbance of the hydrated electron beyond 0.6 ps whose reactivity is negligible up to 1ps. Therefore, the following relation can be considered:

$$\Delta A(r, t = 1\text{ps}) = L\epsilon_{800}[\mathrm{e}^-_{\mathrm{hyd}}]_{t=1\mathrm{ps}}(r) = L\epsilon_{800}\eta_{\mathrm{I}}\eta_{\mathrm{S}}\mathrm{MRCP}(r) \quad (12)$$

where $\eta_{\mathrm{I}}$ and $\eta_{\mathrm{S}}$ are the quantum yields of ionization per absorbed photon and electron solvation per water ionization, respectively (Figure 1). In Appendix III, we demonstrate the following relation between the measured transient absorbance and the MRCP at $r = 0$:

$$\Delta A_{\mathrm{mes}} = (0.92 \pm 0.01)L\epsilon_{800}\eta_{\mathrm{I}}\eta_{\mathrm{S}}\mathrm{MRCP}(0) \quad (13)$$

Given the measured maximum transient absorbance ($\Delta A_{\mathrm{mes}} = 1.1$, Figure 3b), the molar extinction coefficient of the hydrated electron at 800 nm ($\epsilon_{800} = 15\,700$ mol$^{-1}$ dm$^3$ cm$^{-1}$),[10,11] and the MRCP at $r = 0$, (MRCP(0) = 0.042 mol dm$^{-3}$), we deduce the quantum yield of formation of the hydrated electron per absorbed photon: $\eta_{\mathrm{I}}\eta_{\mathrm{S}} = 0.26$. From the value of the MLCP at $z = 0$, (MLCP(0) = 0.59 mol dm$^{-3}$), the maximum concentration of photogenerated hydrated electron at the entrance of the excited sample is thus $[\mathrm{e}^-_{\mathrm{hyd}}]_{\mathrm{max}} = \eta_{\mathrm{I}}\eta_{\mathrm{S}}\mathrm{MLCP}(0) = 0.15$ M. Such an extremely high concentration of hydrated electron has never been reported in photolysis or radiolysis experiments.

Now, let us compare our quantum yield of formation of the hydrated electron to the values obtained in the literature. Nikogosyan et al.,[6] using transient spectroscopic measurement in the time domain $10^{-11} - 10^{-9}$ s, have reported a quantum yield of formation of the hydrated electron of 0.15 per absorbed

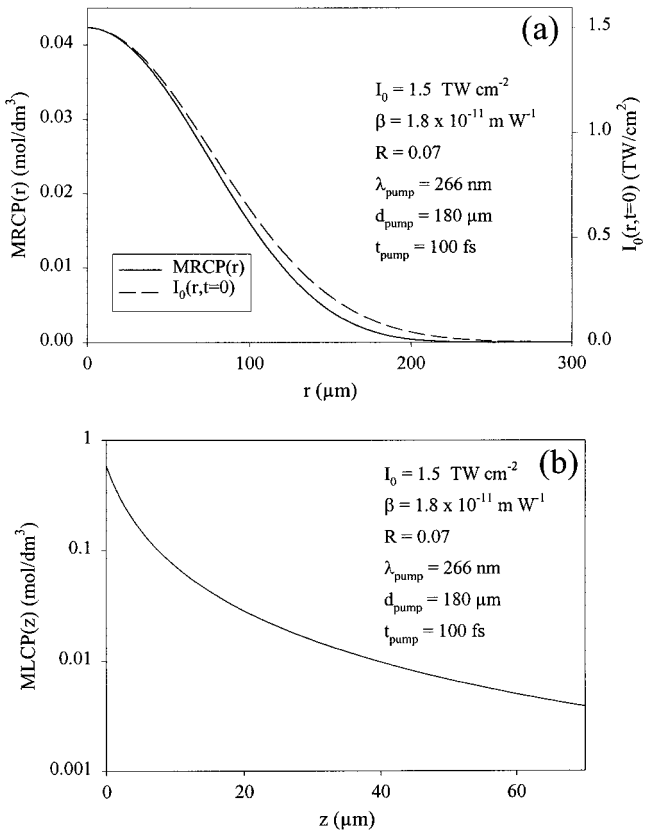


**Figure 6.** Absorbed photon concentration profiles for a two-photon absorption inside the water jet. (a) Mean radial concentration profile MRCP*(r)* and input pulse spatial profile $I_0(r,t = 0)$. (b) Maximum longitudinal concentration profile MLCP(z), according to eqs 4 and 10 (see text).

photon at 266 nm. However, this value is an underestimate because they do not take into account the geminate recombination occurring within the first nanosecond.[8,9] As proposed elsewhere,[13,41] this 0.15 value should be divided by the probability to escape the geminate recombination (0.45).[8] Therefore, the initial quantum yield of formation of the hydrated electron per absorbed photon in the experiments of Nikogosyan et al.[6] should be 0.33. Recently, Bartels and Crowell,[41] using the conductivity jump method, measured the escaped solvated electron yield following two-photon excitation of water at 266 nm. Taking into account the geminate recombination, they determined the initial quantum yield of formation of the hydrated electron per absorbed photon to be 0.24.[42] Our 0.26 value is in close agreement with this latter value.

## Concluding Remarks

From the measured SB-TPA coefficient at 266 nm, we calculated the energy deposition as a function of depth using eq 9 and estimated that most of the energy was actually absorbed in the first 10 micrometers of the water jet (Figure 6). This result is in agreement with experiments performed using a 500 $\mu$m thick water jet, for which the measured signal was the same as that obtained with the 70 $\mu$m thick water jet. Consequently, we estimated that the maximum local concentration of the hydrated electron is close to 0.15 M. This concentration corresponds to one electron per sphere of 14 Å radius on average. Estimations of the ionization/dissociation ($\eta_I/\eta_D$) branching ratio are between 1.2[6] and 1.8[9] (Figure 1). Let us assume that this ratio is 1.5 and is independent of the laser intensity. Then, in a sphere of 20 Å radius, there are two H atoms, three hydronium cations, five hydroxyl radicals, and three hydrated electrons, i.e., on average, a total of 13 radicals, a peak concentration of radicals of 0.6 M. Given the diffusion coefficient ($D(e^-_{hyd}) = 5 \times 10^{-9}$ m$^2$ s$^{-1}$)[2], during 300 ps (Figure 3a), the hydrated electron may diffuse along a mean distance of 12.2 Å. So an hydrated electron could react not only with its two parent radicals ($H_3O^+$ and OH$^\bullet$) but also with the 10 other radicals present in the same sphere of 20 Å radius since all the chemical species involved may also diffuse and their diffusion coefficient are comparable. A crude analysis of the observed kinetics (Figure 4) can be done assuming that all the generated radical species (0.6 M) react with each other with a second-order rate constant of $5 \times 10^9$ dm$^3$ mol$^{-1}$ s$^{-1}$; such a crude analysis[43] would give a half-life of about 300 ps for the hydrated electron, which is in agreement with the experimental data. From our previous work,[23] we estimate the average concentration of the hydrated electron at 1 ns along the jet after a 1.5 TW/cm$^2$ excitation at 266 nm to $1.6 \times 10^{-3}$ M, which can be compared with the value obtained at 1 ps ($10^{-2}$ M) within the same experimental conditions. Therefore, in our experimental conditions, the survival probability of the hydrated electron at 1 ns is only 0.16 ± 0.02. This value is almost 3 times smaller than the probability of escaping the geminate recombination (0.45).[8] This behavior cannot be described within the theoretical framework developed for the geminate recombination.[15]

Finally, we observed water vapor formation around the jet, and we heard a noise due to the laser induced volume expansion and/or vaporization. Moreover, after a few microseconds, the laser analyzing light was no longer transmitted through the water jet due to light scattering. These phenomena might be a consequence of H atom formation at very high concentration (0.1 M) inducing a significant production of $H_2$. Such a high concentration implies a drastic volume expansion in the microsecond time scale as observed and already reported for other liquids.[44]

The development of such studies opens a new route toward the understanding of electron hydration and reactivity inside radiolytic spurs,[1−3] which differ significantly from those occurring in dilute aqueous solution.

**Acknowledgment.** The authors are thankful to G. Vigneron, R. Haïdar, and S. Buguet for their help on the laser system and the acquisition routines.

## Appendix I: Estimation of the error on the SB-TPA Coefficient

The peak intensity is calculated from the pulse energy using eq 5. The error on the calculated peak intensity is thus:

$$\frac{\Delta I_0}{I_0} = \frac{\Delta E_0}{E_0} + \frac{\Delta t_0}{t_0} + 2\frac{\Delta d_0}{d_0} \qquad \text{(A.I.1)}$$

Since the experimental errors on the energy measurements are small compared to the errors on the pulse duration (±10%) and the spatial profile (±5%), the error on the peak power intensity is thus ±20%. Using eqs 5 and 6, the derivative of the transmittance with respect to the input pulse energy can be written as

$$T'(E) = \frac{\partial T}{\partial E_0}(E) = -\frac{\beta_2 L(1-R)^3}{{E_0}^2}\int_0^\infty 2\pi r\,\mathrm{d}r \int_{-\infty}^{\infty} \mathrm{d}t \frac{{I_0}^2(r,t)}{[1+\beta_2 L(1-R) I_0(r,t)]^2} \qquad \text{(A.I.2)}$$

The tuning of the energy of the input pulse enables the experimental measurement of the transmittance. For small input power intensities (small pulse energies), using eq 4, equation A.I.2 can be approximated by

$$T'(E) = -\frac{L\beta_2(1-R)^3}{2\sqrt{2}}\frac{I_0}{E_0} \quad \text{(A.I.3)}$$

Using eq A.I.3, a relationship between the errors on the peak power intensity and the SB-TPA coefficient can be derived:

$$\frac{\Delta\beta_2}{\beta_2} = \frac{\Delta I_0}{I_0} \quad \text{(A.I.4)}$$

The relative error on the calculated determination of the SB-TPA coefficient is thus ± 20%.

## Appendix II: Relation between the SB-TPA Coefficient and TB-TPA Spectrum

The induced absorbance due to a TPA absorption is related to the TB-TPA coefficient as follows:[35]

$$\Delta A(\lambda_{\text{probe}}) \approx \frac{2I_0^{\text{pump}}L}{\ln(10)}\sqrt{\frac{\lambda_{\text{pump}}}{\lambda_{\text{probe}}}}\beta_{\text{pump,probe}}(1-R_{\text{pump}}) \quad \text{(A.II.1)}$$

where $\lambda_{\text{probe}}$ and $\lambda_{\text{pump}}$ are the wavelengths of the probe and pump pulse respectively, $L$ is the sample thickness, $I_0^{\text{pump}}$ the intensity of the pump pulse before the sample, $R_{\text{pump}}$ the Fresnel loss at the sample interface for the pump wavelength, and $\beta_{\text{pump,probe}}$ the TB-TPA coefficient. Here, we neglect the time dependency because this will complicate the equations without changing the final result. Furthermore, it will considered thereafter that both pulses (pump and probe) are linearly polarized and have parallel polarization directions.

Replacing $\beta_{\text{pump,probe}}$ by its expression as a function of the third-order susceptibility[35,34] $\chi^{(3)}$, the ratio of the absorbances for two different probe wavelengths $\lambda_1$ and $\lambda_2$, and a fixed pump wavelength $\lambda_1$ can be expressed as

$$\frac{\Delta A(\lambda_1)}{\Delta A(\lambda_2)} = \frac{\lambda_2}{\lambda_1}\frac{n_2}{n_1}\frac{\text{Im}(\chi^{(3)}_{\lambda_1,\lambda_1})}{\text{Im}(\chi^{(3)}_{\lambda_1,\lambda_2})} \quad \text{(A.II.2)}$$

where $n_i$ is the refractive index at the wavelength $\lambda_i$. The ratio of the SB-TPA coefficients for two different wavelengths $\lambda_1$ and $\lambda_3$ can also be expressed as a function of the third-order susceptibility:[34,35]

$$\frac{\beta_{\lambda_1,\lambda_1}}{\beta_{\lambda_3,\lambda_3}} = \frac{\lambda_3}{\lambda_1}\left(\frac{n_3}{n_1}\right)^2\frac{\text{Im}(\chi^{(3)}_{\lambda_1,\lambda_1})}{\text{Im}(\chi^{(3)}_{\lambda_3,\lambda_3})} \quad \text{(A.II.3)}$$

The combination of eqs A.II.2 and A.II.3 gives the relation between the TB-TPA spectrum and the SB-TPA coefficient:

$$\frac{\Delta A(\lambda_1)}{\Delta A(\lambda_2)} = \frac{\lambda_2}{\lambda_3}\frac{n_1 n_2}{{n_3}^2}\frac{\text{Im}(\chi^{(3)}_{\lambda_3,\lambda_3})}{\text{Im}(\chi^{(3)}_{\lambda_1,\lambda_2})}\frac{\beta_{\lambda_1,\lambda_1}}{\beta_{\lambda_3,\lambda_3}} \quad \text{(A.II.4)}$$

This equation is of interest when both sides refer to the same electronic transition, i.e., when $\lambda_3 = 2\lambda_1\lambda_2/(\lambda_1+\lambda_2)$. For this particular case, eq A.II.4 becomes

$$\frac{\Delta A(\lambda_1)}{\Delta A(\lambda_2)} = \frac{\lambda_1+\lambda_2}{2\lambda_1}\frac{n_1 n_2}{{n_3}^2}\frac{\text{Im}(\chi^{(3)}_{\lambda_3,\lambda_3})}{\text{Im}(\chi^{(3)}_{\lambda_1,\lambda_2})}\frac{\beta_{\lambda_1,\lambda_1}}{\beta_{\lambda_3,\lambda_3}} \quad \text{(A.II.5)}$$

The first and second factors of the right-hand side of equation A.II.5 are almost unity if the wavelengths are close enough. The third factor is unknown but can be approximated under certain conditions. When the beams polarization are linear and parallel, the two-third-order susceptibilities are then similar. We thus have at the first-order the approximate relation:

$$\xi = \frac{\Delta A(\lambda_1)}{\Delta A(\lambda_2)}\frac{\beta_{\lambda_3,\lambda_3}}{\beta_{\lambda_1,\lambda_1}} \approx 1 \quad \text{(A.II.6)}$$

## Appendix III: Relation between the Measured Optical Density and the Mean Radial Concentration Profile

In this appendix, we establish a relation between the optical density measured with a beam of definite transverse size and the mean radial concentration profile as defined in eqs 9−11. It is supposed that the induced absorption is infinitely long-lived compared to the pump and probe pulses. Both pump and probe pulses are assumed to be Gaussian in space and to be centered with respect to each other. It is also considered that they propagate through the sample without any deformation. The incident fluency of the probe pulse is

$$E^{\text{probe}}(r) = E_0^{\text{probe}}\frac{4\ln 2}{\pi d_{\text{probe}}^2}\exp\left(-\frac{4\ln 2 r^2}{d_{\text{probe}}^2}\right) \quad \text{(A.III.1)}$$

The induced absorbance defined in eq 12 can be rewritten as

$$\Delta A(r,t{=}1\text{ps}) = \Delta A_{\max}\frac{\text{MRCP}(r)}{\text{MRCP}(0)} \quad \text{(A.III.2)}$$

The transmitted energy of the probe pulse propagating one picosecond after the pump pulse is thus

$$E(r,t{=}1\text{ps}) = (1-R_{\text{probe}})^2 E^{\text{probe}}(r)10^{-\Delta A(r,t=1\text{ps})} \quad \text{(A.III.3)}$$

where $R_{\text{probe}}$ is the Fresnel loss of the probe pulse at the air−sample interfaces. Using eq A.III.2 and integrating over the transverse plane, one obtains

$$E(t{=}1\text{ps}) = (1-R_{\text{probe}})^2\int_0^\infty 2\pi r E^{\text{probe}}(r)\times \exp\left(-\ln(10)\frac{\text{MRCP}(r)}{\text{MRCP}(0)}\Delta A_{\max}\right)\text{d}r \quad \text{(A.III.4)}$$

Finally, the measured absorbance is

$$\Delta A_{\text{mes}} = \log_{10}\left(\frac{(1-R_{\text{probe}})^2 E_0^{\text{probe}}}{E(t{=}1\text{ps})}\right) = -\log_{10}\left(\int_0^\infty 2\pi r\frac{4\ln 2}{\pi d_{\text{probe}}^2}\exp\left(-\frac{4\ln 2 r^2}{d_{\text{probe}}^2}\right)\times \exp\left(-\ln(10)\frac{\text{MRCP}(r)}{\text{MRCP}(0)}\Delta A_{\max}\right)\text{d}r\right) \quad \text{(A.III.5)}$$

For the numerical values used in the present work ($d_{\text{probe}} = 50$ $\mu$m, $d_{\text{pump}} = 180$ $\mu$m, $\beta = 1.8\times10^{-11}$ m/W, $R = 0.07$, $0 < \Delta A_{\max} < 2$, $I_0 = 1.5$ TW/cm$^2$), this complex expression is well approximated by the following relation:

$$\Delta A_{mes} = (0.92 \pm 0.01)\Delta A_{max} = (0.92 \pm 0.01)L\epsilon_{800}\eta_I\eta_S \mathrm{MRCP}(0) \quad \text{(A.III.6)}$$

In this expression, the error bars reflect the dependency of the factor when $\Delta A_{max}$ is varied from 0.1 to 2.0.

## References and Notes


(1) Hart, E. J.; Anbar, M. *The Hydrated Electron*; Wiley Interscience: New York, 1970.

(2) Tabata, Y.; Ito, Y.; Tagawa, S. *Handbook of Radiation Chemistry*; CRC Press: Boston, 1991.

(3) Mozumder, A. *Fundamentals of Radiation Chemistry*; Academic Press: New York, 1999.

(4) Bronskill, M. J.; Wolff, R. K.; Hunt, J. W. *J. Phys. Chem.* **1969**, *73*, 1175.

(5) Jonah, C. D.; Matheson, M. S.; Miller, J. R.; Hart, E. J. *J. Phys. Chem.* **1976**, *80*, 1267.

(6) Nikogosyan, D. N.; Oraevsky, A. A.; Rupasov, V. I. *Chem. Phys.* **1983**, *77*, 131.

(7) Migus, A.; Gauduel, Y.; Martin, J. L.; Antonetti, A. *Phys. Rev. Lett* **1987**, *58*, 1559.

(8) Crowell, R. A.; Bartels, D. M. *J. Phys. Chem.* **1996**, *100*, 17940.

(9) Thomsen, C. L.; Madsen, D.; Keiding, S. R.; Thogersen, J.; Christiansen, O. *J. Chem. Phys.* **1999**, *110*, 3453.

(10) Michael, B. D.; Hart, E. J.; Schmidt, K. H. *J. Phys. Chem.* **1971**, *75*, 2798.

(11) Jou, F.-Y.; Freeman, G. R. *J. Phys. Chem.* **1979**, *83*, 2383.

(12) Gauduel, Y.; Pommeret, S.; Migus, A.; Antonetti, A. *J. Phys. Chem.* **1993**, *93*, 3880.

(13) Reuther, A.; Laubereau, A.; Nikogosyan, D. N. *J. Phys. Chem.* **1996**, *100*, 16794.

(14) Buxton, G. V.; Greenstock, C. L.; Helman, W. P.; Ross, A. B. *J. Phys. Chem. Ref. Data* **1988**, *17*, 513.

(15) Pimblott, S. M. *J. Phys. Chem.* **1991**, *95*, 6946.

(16) Goulet, T.; Jay-Gerin, J. P. *J. Chem. Phys.* **1992**, *96*, 5076.

(17) The Notre Dame Radiation Laboratory Radiation Chemistry Data Center (http://allen.rad.nd.edu) provides a large set of references on radiation chemistry reaction rates.

(18) Gauduel, Y.; Pommeret, S.; Migus, A.; Yamada, N.; Antonetti, A. *J. Opt. Soc. Am., B* **1990**, *7*, 1528.

(19) Aldrich, J. E.; Bronskill, M. J.; Wolf, R. K.; Hunt J. W. *J. Chem. Phys.* **1971**, *55*, 530.

(20) Duplâtre, G.; Jonah, C. D. *Radiat. Phys. Chem.* **1985**, *24*, 57.

(21) Wolff, R. K.; Bronskill, M. J.; Hunt, J. W. *J. Chem. Phys.* **1975**, *7*, 317.

(22) Pimblott, S. M.; LaVerne, J. A. *J. Phys. Chem. A* **1998**, *102*, 2967.

(23) Gobert, F.; Pommeret, S.; Vigneron, G.; Buguet, S.; Haidar, R.; Mialocq, J.-C.; Lampre, I.; Mostafavi, M. *Res. Chem. Intermed.* **2001**, *27*, 901.

(24) Pommeret, S.; Gobert, F.; Mostafavi, M.; Lampre, I.; Pernot, P.; Haidar, R.; Buguet, S.; Vigneron, G.; Mialocq, J.-C. In *Ultrafast Phenomena XII*; Elsaesser, T., Mukamel, S., Murnane, M. M., Scherer, N. F., Eds.; Springer Series in Chemical Physics; Springer: New York, 2000; Vol. 66, p 536.

(25) Pommeret, S.; Naskrecki, R.; van der Meulen, P.; Ménard, M.; Vigneron, G.; Gustavsson, T. *Chem. Phys. Lett.* **1998**, *288*, 833.

(26) Naskrecki, R.; Ménard, M.; van der Meulen, P.; Vigneron, G.; Pommeret, S. *Opt. Comm.* **1998**, *153*, 32.

(27) Fournier, T.; Pommeret, S.; Mialocq, J.-C.; Deflandre, A.; Rozot, R. *Chem. Phys. Lett.* **2000**, *325*, 171.

(28) Mialocq, J.-C.; Sutton, J.; Goujon, P. *J. Chem. Phys.* **1980**, *72*, 6338.

(29) Lam, K. Y.; Hunt, J. W. *J. Phys. Chem.* **1975**, *79*, 317.

(30) Jonah, C. D.; Miller, J. R.; Matheson, M. S. *J. Phys. Chem.* **1977**, *81*, 931.

(31) Gauduel, Y.; Pommeret, S.; Migus, A.; Yamada, N.; Antonetti, A. *J. Am. Chem. Soc.* **1990**, *112*, 2925.

(32) Pastina, B.; LaVerne, J. A.; Pimblott, S. M. *J. Phys. Chem. A* **1999**, *103*, 5841.

(33) Kee, T. W.; Hee Son, D.; Kambhampati, P.; Barbara, P. F. *J. Phys. Chem. A* **2001**, *105*, 8434.

(34) Shen, Y. R. *The Principle of Nonlinear Optics*; Wiley: New York, 1984.

(35) Sutherland, R. L. *Handbook of Nonlinear Optics*; Marcel Dekker: New York, 1996.

(36) The fitted value of $R$ is quite large compare to the calculated value with the refractive indexes (0.03). This discrepancy is due to the surface roughness of the jet that induces additional diffusion.

(37) Selden, A. C. *Science* **1971**, *229*, 210.

(38) Keelly, P. J.; Jones, S. C.; Shen, X. A.; Simpson, L.; Braunlich, P. F.; Casper, R. T. *Phys. Rev. B* **1990**, *42*, 11370.

(39) Catalano, I. M.; Cingolani, A. *Solid State Commun.* **1984**, *52*, 539.

(40) Catalano, I. M.; Cingolani, A. *J. Appl. Phys.* **1978**, *50*, 5638.

(41) Bartels, D. M.; Crowell, R. A. *J. Phys. Chem. A* **2000**, *104*, 3349.

(42) As pointed out in ref 41, it is important to define the quantum yield in terms of hydrated electron produce per one photon. This definition is used throughout the present paper. In ref 41, the authors used the quantum efficiency rather than the quantum yield. Consequently, their values of quantum efficiency at 266 nm should be divided by two to be compared with our value and those of ref 6.

(43) This is an approximation: one really cannot consider it as a simple second-order system because, for example, $H^+$ does not react with $H^\bullet$.

(44) Tsuboi, Y.; Hatanaka, K.; Fukumara H.; Masuhara, H. *J. Phys. Chem. A* **1998**, *102*, 1661.